



GLOBAL JOURNAL OF RESEARCHES IN ENGINEERING: E
CIVIL AND STRUCTURAL ENGINEERING
Volume 15 Issue 2 Version 1.0 Year 2015
Type: Double Blind Peer Reviewed International Research Journal
Publisher: Global Journals Inc. (USA)
Online ISSN: 2249-4596 & Print ISSN: 0975-5861

Stochastic Finite Element Analysis for Transport Phenomena in Geomechanics using Polynomial Chaos

By S. Drakos & G. N. Pande

International Center for Computational Engineering, Greece

Abstract- Transport Phenomena in Geomechanics occur under uncertain conditions and their parameters dominated by spatial randomness. The prediction of the progress of these phenomena is a stochastic problem rather than a deterministic. To solve the problem a procedure of conducting Stochastic Finite Element Analysis using Polynomial Chaos is presented. It eliminates the need for a large number of Monte Carlo simulations thus reducing computational time and making stochastic analysis of practical problems feasible. This is achieved by polynomial chaos expansion of the concentration. An example of a pollution development in a soil is presented and the results are compared to those obtained from Random Finite Element Analysis. A close matching of the two is observed.

GJRE-E Classification : FOR Code: 290704



Strictly as per the compliance and regulations of :



© 2015. S. Drakos & G. N. Pande. This is a research/review paper, distributed under the terms of the Creative Commons Attribution-Noncommercial 3.0 Unported License (<http://creativecommons.org/licenses/by-nc/3.0/>), permitting all non commercial use, distribution, and reproduction in any medium, provided the original work is properly cited.

Stochastic Finite Element Analysis for Transport Phenomena in Geomechanics using Polynomial Chaos

S. Drakos^α & G. N. Pande^σ

Abstract- Transport Phenomena in Geomechanics occur under uncertain conditions and their parameters dominated by spatial randomness. The prediction of the progress of these phenomena is a stochastic problem rather than a deterministic. To solve the problem a procedure of conducting Stochastic Finite Element Analysis using Polynomial Chaos is presented. It eliminates the need for a large number of Monte Carlo simulations thus reducing computational time and making stochastic analysis of practical problems feasible. This is achieved by polynomial chaos expansion of the concentration. An example of a pollution development in a soil is presented and the results are compared to those obtained from Random Finite Element Analysis. A close matching of the two is observed.

I. INTRODUCTION

The Transport phenomena in geomechanics is a complex problem and cover a wide range of application. Problem as the contamination of land in many countries or recovery of oil in reservoir e.t.c, are dominated from the uncertainty and spatial variability of the properties of soil materials. Various forms of uncertainties arise which depend on the nature of geological formation, the extent of site investigation, the type and the accuracy of design calculations etc. In recent years there has been considerable interest amongst engineers and researchers in the issues related to quantification of uncertainty as it affects safety, design as well as the cost of projects.

Zhang, P. and Hu, L. (2014) presented in their study, a generalized model of preferential flow paths based on a dual-domain model which reflects contaminant transport and the dynamic transfer between two domains, and quantitatively analyzes the difference between advection-dispersion model (ADM) and dual-domain mass transfer model (DDM) in pore scale. Basic idea of this paper was the complexity of contaminant transport through highly heterogeneous soil on predicting pollution of the soil and groundwater system. Mousavi et al (2013) presented the development and the application of a numerical model for simulation of

advective and diffusive-dispersive contaminant transport using a stochastic finite-element approach. Employing the stochastic finite-element method proposed in this study, the response variability was reproduced with a high accuracy. Johnson et al (2010) introduced an approach which has been incorporated into a spreadsheet model which uses a one-dimensional solution to the advection dispersion equation, which readily lends itself to Monte Carlo applications. The scope of this work was the definition of contaminant source release of contaminant mass transport simulation in the saturated zone as many sites the release history is unknown. Nadim et al (2004) proposed a three-dimensional stochastic model for the generation and transport of LFG in order to quantify the uncertainties. Using Monte Carlo simulations, multiple realizations of key input parameters was generated. For each realization, LFG transport was simulated and then used to evaluate probabilistically the rates and efficiency of energy recovery. Wörman, A. and Xu, S. (2001) developed a new modeling framework for internal erosion in heterogeneous stratified soils by combining existing methods used to study sediment transport in canals, filtration phenomena, and stochastic processes. The framework was used to study the erosion process in sediments caused by a flow of water through a covering filter layer that deviates from geometrical filter rules. By the use of spectral analysis and Laplace transforms, mean value solutions to the transport rate and the variance about the mean was derived for a transport constraint at the upstream boundary and a constant initial transport.

In this paper we present a general SFEM for transport phenomena in geomechanics using the method of Generalized Polynomial Chaos (GPC). In the first part of the paper a new algorithm based on RFEM using the Circulant Embedding method (Lord et al 2014) is presented in order to generate the random fields. In the second part, development of SFEM based on the Karhunen-Loeve Expansion for stochastic process discretisation and GPC is described. Finally in the last part of the paper, the problem of contamination of soil due to a surface source is solved by the two methods and the results are compared.

*Author α: General Secretary of International Center for Computational Engineering (ICCE), Rhodes Greece.
e-mail: stefanos.drakos@gmail.com*

Author σ: Chairman of International Center for Computational Engineering (ICCE), Rhodes Greece.

a) Problem description and Model formulation

Let us consider a general spatial domain $D \subseteq R^3$ bounded by the surface S. Based on the conservative laws, in the domain, the transport

mechanisms, such as convection (also called advection), diffusion can be described by the following equation:

$$\frac{\partial u(t, \mathbf{x}, \boldsymbol{\omega})}{\partial t} - D_{if}(\mathbf{x}, \boldsymbol{\omega}) \Delta u(t, \mathbf{x}, \boldsymbol{\omega}) + c(\mathbf{x}, \boldsymbol{\omega}) \nabla u(t, \mathbf{x}, \boldsymbol{\omega}) = f(\mathbf{x}, \boldsymbol{\omega}) \text{ in } (0, T] \times D \times \Omega$$

$$u(\mathbf{0}, \mathbf{x}) = u_0 \text{ in } B_D$$
(1)

In order to model the problem assuming the sample space $(\Omega, \mathcal{F}, \mathbb{P})$ where \mathcal{F} the σ - algebra is and is considered to contain all the information that is available, \mathbb{P} is the probability measure. The diffusion and convection coefficient $\{D_{if}(\mathbf{x}, \boldsymbol{\omega}) : \in D \times \Omega\}$ and the source or sink $\{f(\mathbf{x}, \boldsymbol{\omega}) : \in D \times \Omega\}$ considered as second order random fields and their functions are determined $D_{if}, c, f : D \times \Omega \rightarrow \mathbb{R} \in V = L^2(\Omega, L^2(D))$

and characterized by specific distribution. The Gaussian distribution is the default distribution in most application of probabilistic engineering mechanics. In our case the Gaussian distribution is inappropriate because of coefficients' nature. None of them cannot take negative value. Thus in order to cover all the values of them greater than zero a long normal distribution is adopted.

The expected value of a quantity of the problem is given by the following norm:

$$\|\cdot\|_{L^2(\Omega, L^2(D))} = \int_{\Omega} \int_D |\cdot|^2(\mathbf{x}, \boldsymbol{\omega}) d\mathbf{x} d\mathbb{P} = \mathbb{E}(\|\cdot\|_{L^2(D)})$$
(2)

In essence the solution of the problem is a function of the form $u_t \in \Omega \times D \rightarrow \mathbb{R}$ for every fixed t, i.e. a random field and is not a deterministic function.

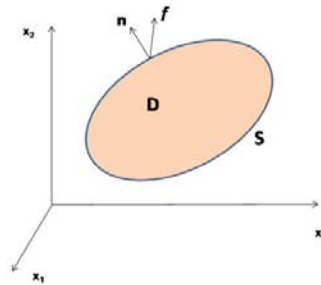


Figure 1 : Spatial Domain D bounded by the surface S

b) Variational Formulation

Using a test function $v \in V_0^h \in V = L^2(\Omega, L^2(D))$ and integrating by parts over the spatial domain $D \subseteq R^3$.

$$\int_D \frac{\partial u(t, \mathbf{x}, \boldsymbol{\omega})}{\partial t} \cdot v(\mathbf{x}) d\mathbf{x} - \int_D D_{if}(\mathbf{x}, \boldsymbol{\omega}) \Delta u(t, \mathbf{x}, \boldsymbol{\omega}) \cdot v(\mathbf{x}) d\mathbf{x} +$$

$$+ \int_D c(\mathbf{x}, \boldsymbol{\omega}) \nabla u(t, \mathbf{x}, \boldsymbol{\omega}) \cdot v(\mathbf{x}) d\mathbf{x} = \int_D f(\mathbf{x}, \boldsymbol{\omega}) \cdot v(\mathbf{x}) d\mathbf{x}$$
(3)

Considering the boundary condition

$$\int_D \frac{\partial u(t, \mathbf{x}, \boldsymbol{\omega})}{\partial t} \cdot v(\mathbf{x}) d\mathbf{x} = \int_D D_{if}(\mathbf{x}, \boldsymbol{\omega}) \nabla u(t, \mathbf{x}, \boldsymbol{\omega}) \cdot \nabla v(\mathbf{x}) d\mathbf{x} -$$

$$- \int_D c(\mathbf{x}, \boldsymbol{\omega}) \nabla u(t, \mathbf{x}, \boldsymbol{\omega}) \cdot v(\mathbf{x}) d\mathbf{x} - \int_D f(\mathbf{x}, \boldsymbol{\omega}) \cdot v(\mathbf{x}) d\mathbf{x}$$
(4)

II. RANDOM FINITE ELEMENT

The most common way to solve this problem is to create a random field of the soil properties which is mapped to a grid of finite element and then for different every time realization of the fields $\{D_{if}(\mathbf{x}, \boldsymbol{\omega}) : \in D \times \Omega\}$ $\{c(\mathbf{x}, \boldsymbol{\omega}) : \in D \times \Omega\}$ and the source or sink $\{f(\mathbf{x}, \boldsymbol{\omega}) : \in D \times \Omega\}$ to solve an ordinary boundary value problem using the Monte Carlo method. Assuming the same randomness for all leads to computational efficiency and is not far from the reality.

In the current work the random field is generated by the Circulant Embedding method (Lord et

all 2014) using the Fast Fourier Algorithm resulting, as will be shown in the following sections, an exact simulation of stochastic processes.

Following the random field generation the displacement field $u_k(\mathbf{x})$ for each realization is taken place. At the end of all running the statistical moment based on the Monte Carlo method is calculated. The problem for each realization of $\{D_{if}(\mathbf{x}, \boldsymbol{\omega}) : \in D \times \Omega\}$ and the source or sink $\{f(\mathbf{x}, \boldsymbol{\omega}) : \in D \times \Omega\}$ is:

$$\int_D \frac{\partial u_k(\mathbf{x}, \boldsymbol{\omega})}{\partial t} \cdot v(\mathbf{x}) dx = \int_D D_{if}(\mathbf{x}, \boldsymbol{\omega}) \nabla u_k(\mathbf{x}, \boldsymbol{\omega}) \cdot \nabla v(\mathbf{x}) dx - \int_D c(\mathbf{x}, \boldsymbol{\omega}) \nabla u_k(\mathbf{x}, \boldsymbol{\omega}) \cdot v(\mathbf{x}) dx - \int_D f(\mathbf{x}, \boldsymbol{\omega}) \cdot v(\mathbf{x}) dx \tag{5}$$

And the expected values at the end:

$$\mathbb{E}(u(\mathbf{x})) = \frac{1}{K} \sum_{k=1}^K u_k(\mathbf{x}) \tag{6}$$

And the variance

$$Var(u(\mathbf{x})) = \frac{1}{K-1} \sum_{k=1}^K (u_k(\mathbf{x}) - \mathbb{E}(u(\mathbf{x})))^2 \tag{7}$$

III. RANDOM FIELD GENERATION

The Circulant Embedding method (Lord et al 2014) is a technique used for the generation of realizations of Gaussian stochastic processes. This technique has two main advantages among others. The first is that the statistical properties of the generated process are exactly the same process that we aim. The second advantage arises from the Fast Fourier Transform Algorithm which significantly reduces the computational cost. This method seems to have initially been studied in problems of one dimension by Davies & Harte (1987) and more systematically by Dembo et al. (1989), Dietrich & Newsam (1993, 1997), Gneiting (2000), Stein (2001), Craigmile (2003), and Percival (2006). Extension of the method to a multi-parameter problems studied by Wood (1999), Helgason et al. (2011) whereas in random fields by Dietrich & Newsam (1993), Wood & Chan (1994, 1997), Stein (2002, 2012), Gneiting et al. (2006). Considerable work was recently featured by Lord et al (2014) whose principles are followed in this work. According to the method, in the case where the samples are uniformly distributed in space in a two-dimensional problem, then the covariance matrix C is

Toeplitz (Appendix A) and has as elements Toeplitz blocks (block Toeplitz with Toeplitz blocks (BTTB)). The covariance matrix can be described by the Fast Fourier Algorithm:

$$C = FDF^H \tag{8}$$

Where:

$$F_{N=n_1 n_2 \times n_1 n_2} = F_1 \otimes F_2 \tag{9}$$

The F_1, F_2 are the Fourier matrices with dimension of $n_1 \times n_1$ and $n_1 \times n_2$ respectively and the diagonal matrix D includes the eigenvalues of the covariance matrix. For the application of the method the covariance matrix has to be circulant and for that reason using the BTTB matrix invokes a new circulant ((Appendix A)) matrix is created with n_2 blocks of circulant matrices $n_1 \times n_1$ which is represented uniquely by the reduced matrix $C_{red} = [c_0, \dots, c_{n_2-1}]$. The latter can be replaced uniquely by the vector $c_{red} \in \mathbb{R}^{n_1 n_2}$.

Following the process described and provided that the covariance matrix has non-negative and real eigenvalues we get:

$$Z = D^{1/2} \xi \mu \epsilon \xi \sim N(0, 2I_N) \tag{10}$$

And finally

$$Z = X + iY \tag{11}$$

Considering the covariance matrix:

$$C(x, y) = \sigma^2 \exp\left(-\frac{|x_j - x_i|}{\lambda_x} - \frac{|y_j - y_i|}{\lambda_y}\right) \tag{12}$$

Where:

$$\begin{aligned} X &\sim N(0, C) \\ Y &\sim N(0, C) \end{aligned}$$

In Figures 3 to 6, examples of random fields realization for different correlation lengths of covariance above matrix are presented.

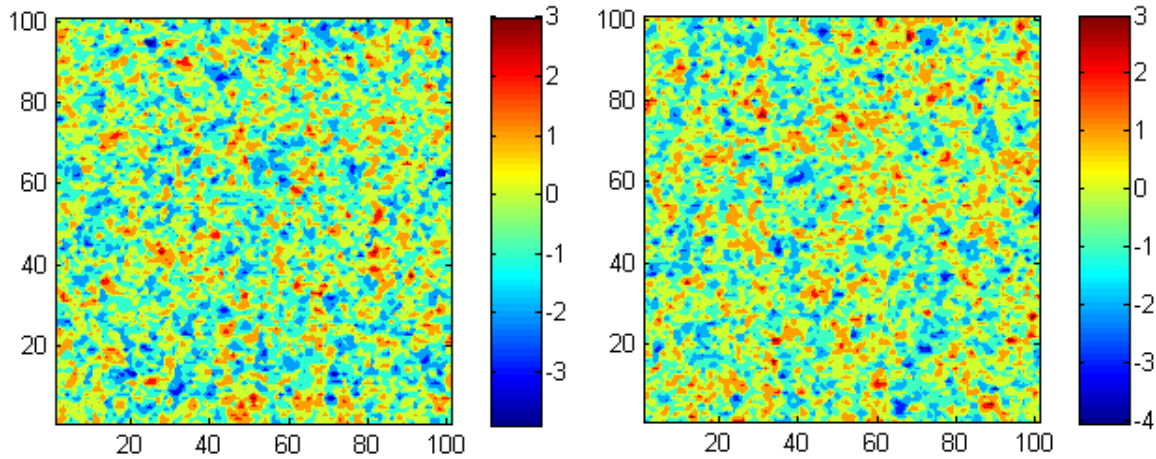


Figure 2 : Random field with dimension $D = [0,100] \times [0,100]$ and correlation length $\lambda_x = \lambda_y = \frac{1}{10}$

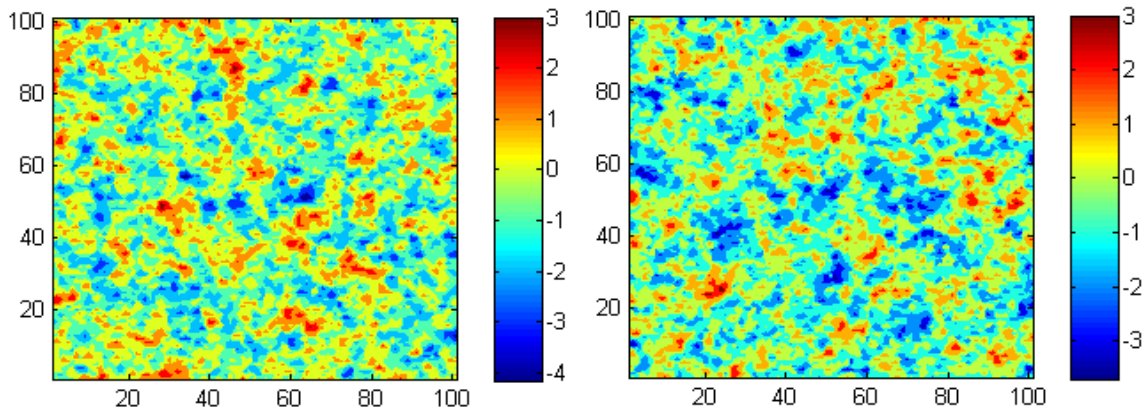


Figure 3 : Random field with dimension $D = [0,100] \times [0,100]$ and correlation length $\lambda_x = \lambda_y = \frac{2}{10}$

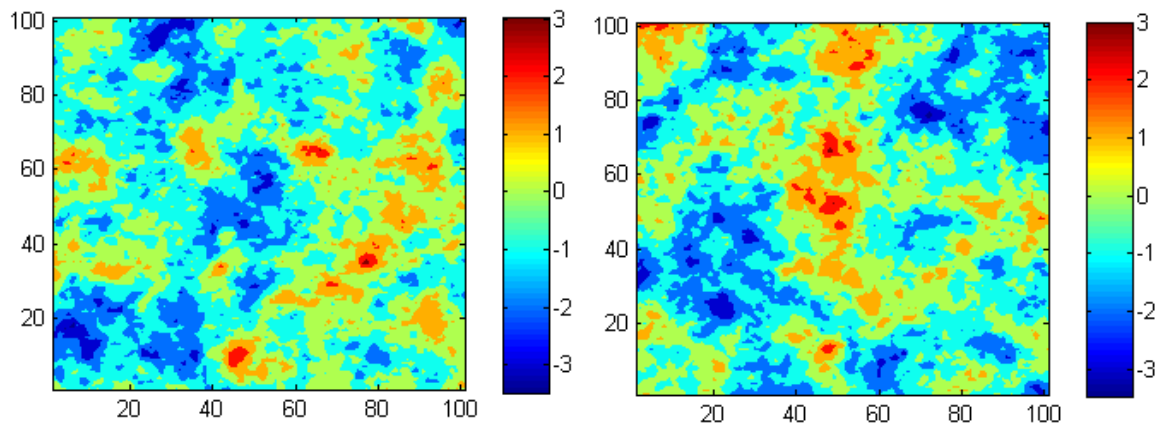


Figure 4 : Random field with dimension $D = [0,100] \times [0,100]$ and correlation length $\lambda_x = \lambda_y = 1$

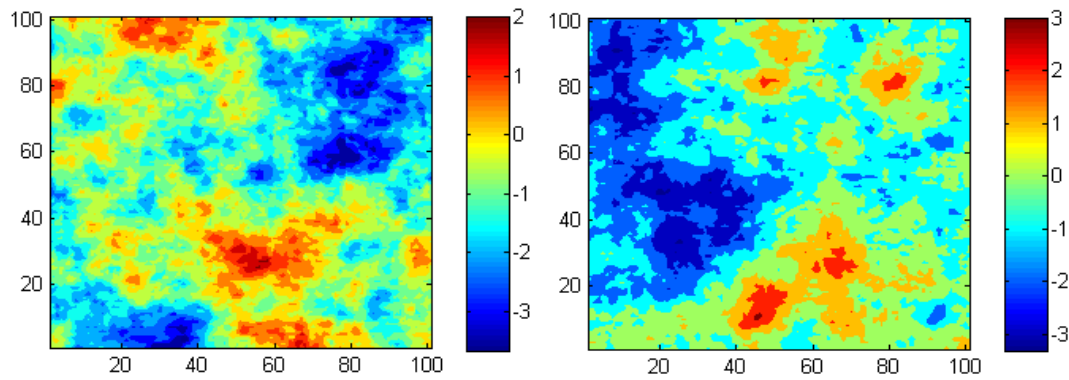


Figure 5 : Random field with dimension $D = [0,100] \times [0,100]$ and correlation length $\lambda_x = \lambda_y = 2$

IV. THE STOCHASTIC FINITE ELEMENT METHOD (SFEM)

The SFEM based on Polynomial Chaos introduced anallatocally by Ghanem & Spanos (1991) and have a wide range of applications and are used to solve problems in various branches of science. In the following paragraphs we introduce the procedure to solve the problems in Geomechanics using the Stochastic Finite Element Method for transport phenomena based on Generalized Polynomial Chaos (Xiu & Karniadakis 2003).

a) Karhunen-Loeve Expansion

One of the major points of the SFEM is the separation of deterministic part from the stochastic part

$$D_{if}(\mathbf{x}, \xi(\omega)) = \exp(\widetilde{D}_{if}(\mathbf{x}) + \sum_{\kappa=1}^{\infty} \sqrt{\lambda_{\kappa}} \varphi_{\kappa} \xi_{\kappa}(\omega))$$

$$c(\mathbf{x}, \xi(\omega)) = \exp(\widetilde{c}(\mathbf{x}) + \sum_{\kappa=1}^{\infty} \sqrt{\lambda_{\kappa}} \varphi_{\kappa} \xi_{\kappa}(\omega))$$
(13)

In practice, calculations were carried out over a finite number of summations (for example 1-5) and the approximate stochastic representation is given by the truncated part of expansion. The number of truncated is coming from the Karhunen-Loeve property where the eigenvalues λ_k decay as the k increase:

$$D_{if}(\mathbf{x}, \xi(\omega)) = \exp(\widetilde{D}_{if}(\mathbf{x}) + \sum_{\kappa=1}^K \sqrt{\lambda_{\kappa}} \varphi_{\kappa} \xi_{\kappa}(\omega))$$

$$c(\mathbf{x}, \xi(\omega)) = \exp(\widetilde{c}(\mathbf{x}) + \sum_{\kappa=1}^k \sqrt{\lambda_{\kappa}} \varphi_{\kappa} \xi_{\kappa}(\omega))$$
(14)

Where:

λ_{κ} : are the eigenvalues of the covariance function

$\varphi_{\kappa}(\mathbf{x})$: are the eigenfunctions of the covariance function $Cov(\mathbf{x}_1, \mathbf{x}_2)$

$\mathbf{x} \in D$ and $\boldsymbol{\omega} \in \Omega$

$\xi = [\xi_1, \xi_1, \dots, \xi_M]: \Omega \rightarrow \Gamma \subset \mathbb{R}^M$ and

$\Gamma = \Gamma_1 \times \Gamma_1 \times \dots \times \Gamma_M$

The pairs of eigenvalues and eigenfunctions arised by the Mercer's theorem:

of the formulation. Thus the method has two types of discretization, the ordinary FEM discretization of geometry and the stochastic discretization of random fields. In the current paper in order to reach in these results the Karhunen-Loeve expansion has been used which is the most efficient method for the discretization of a random field, requiring the smallest number of random variables to represent the field within a given level of accuracy. Based on that the stochastic process of the Diffusion and convection coefficients over the spatial domain with the known mean values \widetilde{D}_{if} and $\widetilde{c}(\mathbf{x})$ and covariance matrix $Cov(\mathbf{x}_1, \mathbf{x}_2)$ is given by:



$$\int_D C(x_1, x_2)\varphi(x_2) = \lambda\varphi(x_1) \quad (15)$$

For two dimensional Domain $D = [-a_1, a_1] \times [-a_2, a_2]$ the eigenvalues are $\lambda_m = \lambda_1\lambda_2$ and eigenfunctions are equal to $\varphi_m(x) = \varphi_1(x_1)\varphi_2(x_2)$ where the values $\{\lambda_1, \lambda_2\}$ and $\{\varphi_1, \varphi_2\}$ calculated by the following equation:

$$\int_D C(x_1, x_2)\varphi_m(x_2) = \lambda_m\varphi_m(x_1), \quad m = 1,2 \quad (16)$$

The rate of eigenvalue decay is inversely proportional to the correlation length. Thus for high correlation length (strong correlation) there is fast decay of the eigenvalues. For small correlation length (weak correlation) we have low decay. For zero correlation length there is not correlation and there is not decay of the eigenvalues. As the correlation length increases the decay rate increasing. If the correlation length is very small i.e correlation length =0.01 then the decay rate is not noticeable.

Implemented the Mercer theorem the first four eigenfunction are presented in figure 6 where in figures 7 and 8 the comparison of initial correlation matrix and the calculated based on the Mercer theorem is shown for different values of variation of diffusion coefficient. In figures 9, 10 The decay of eigenvalues in descending order are presented.

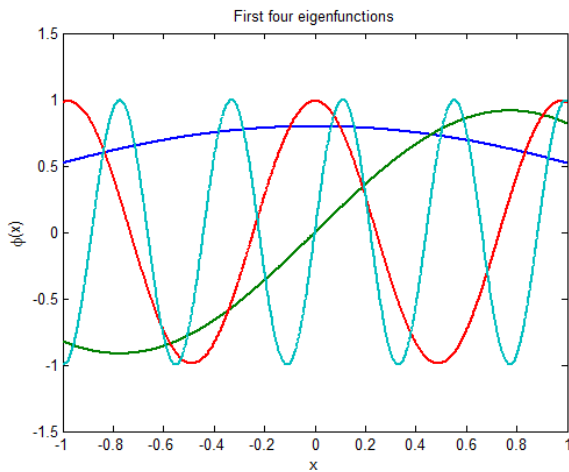


Figure 6 : First four eigenfunctions in the domain $D=[-1,1]$

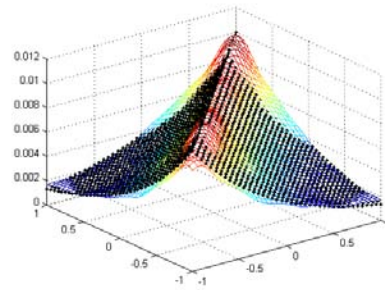


Figure 7 : Comparison of initial covariance matrix and its numerical approach with correlation length=1 and sigma=0.1

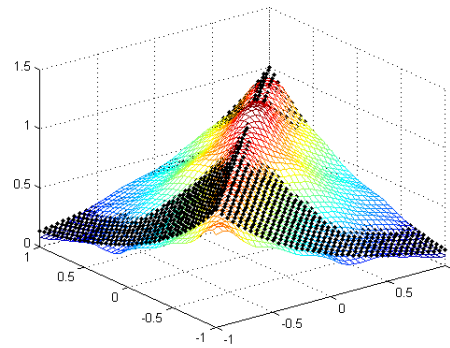


Figure 8 : Comparison of initial covariance matrix and its numerical approach with correlation length=1 and sigma=1

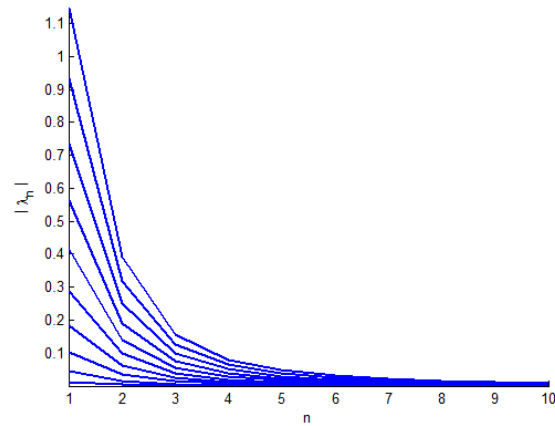


Figure 9 : Eigenvalues decay graph for different variation of diffusion coefficient

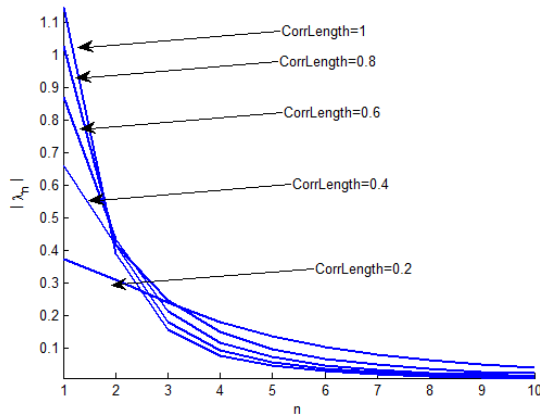


Figure 10 : Eigenvalues decay graph for different values of correlation length

b) Galerkin approximation

The Karhunen-Loeve expansion method enables to replace the calculating procedure for the expected value using instead of the abstract space Ω of random fields ξ their figures and finally to solve a deterministic problem in space $D \times \Gamma \subset \mathbb{R}^M$ instead of space $D \times \Omega$. By performing such replacements in fact a deterministic problem is solved, in contrast to the case of Monte Carlo where a large number of problems carried out. According that the test function of the weak form determined by $v \in L^2_p(\Gamma, H^1_0(D))$ while the solution of the problems in the general form of the boundaries conditions is a function $\tilde{u} \in W = L^2_p(\Gamma, H^1_g(D))$ which is satisfied the equation:

$$\int_D \frac{\partial \tilde{u}(t, \mathbf{x}, \boldsymbol{\omega})}{\partial t} \cdot v(\mathbf{x}) dx = \int_D D_{if}(\mathbf{x}, \boldsymbol{\omega}) \nabla \tilde{u}(t, \mathbf{x}, \boldsymbol{\omega}) \cdot \nabla v(\mathbf{x}) dx - \int_D c(\mathbf{x}, \boldsymbol{\omega}) \nabla \tilde{u}(t, \mathbf{x}, \boldsymbol{\omega}) \cdot v(\mathbf{x}) dx - \int_D f(\mathbf{x}, \boldsymbol{\omega}) \cdot v(\mathbf{x}) dx \tag{17}$$

$$\forall v \in L^2_p(\Gamma, H^1_0(D))$$

The expected value of each side assuming that the behavior of source or sink is deterministic and constant:

$$\begin{aligned} \langle RHS \rangle &= \int_{\Gamma} \rho(y) \int_0^H \frac{\partial \tilde{u}(t, \mathbf{x}, \boldsymbol{\omega})}{\partial t} \cdot v(\mathbf{x}) dx dy \\ \langle LHS \rangle &= \int_{\Gamma} \rho(y) \left[\int_D D_{if}(\mathbf{x}, \boldsymbol{\omega}) \nabla \tilde{u}(t, \mathbf{x}, \boldsymbol{\omega}) \cdot \nabla v(\mathbf{x}) dx - \int_D c(\mathbf{x}, \boldsymbol{\omega}) \nabla \tilde{u}(t, \mathbf{x}, \boldsymbol{\omega}) \cdot v(\mathbf{x}) dx \right] dy \end{aligned} \tag{18}$$

Where:

$\rho : \Gamma \rightarrow \mathbb{R}$ is the η joint density of independent random variables ξ

In order to solve the problem according to the finite element method in the current paper we consider a triangle K with nodes $N_i(x^{(i)}, y^{(i)})$, $i = 1, 2, 3$. To each node N_i there is a hat function φ_i associated, which takes the value 1 at node N_i and 0 at the other two nodes. Each hat function is a linear function on K so it has the form:

$$\varphi_i = a_i + b_i x + c_i y \tag{19}$$

The test v function belongs to the space:

$$V^h = span\{\varphi_1, \varphi_2, \dots, \varphi_N\} \subset H^1_0(D) \tag{20}$$

Any type of higher order shape functions can be used although it will increase the computational cost.

In order to solve the problem of equation 1 we have to create the new space $L^2_p(\Gamma, H^1_0(D))$. For that reason the subspace $S^k \subset L^2_p(\Gamma)$ is considered as (Lord et al 2014).

$$S^k = span\{\psi_1, \psi_2, \dots, \psi_k\} \tag{21}$$

Using the dyadic product of the space V^h , S^k the space $L^2_p(\Gamma, H^1_0(D))$ created. Thus

$$V^{hk} = V^h \otimes V^k = span\{\varphi_i \psi_j, i = 1 \dots N, j = 1, \dots Q\} \tag{22}$$

The space V^{hk} has dimension QN and regards the test function v . In the case where exists N_B finite element supported by boundaries condition then the subspace of solution belongs is:

$$W^{hk} = V^{hk} \oplus span\{\varphi_{N+1}, \varphi_{N+2}, \dots, \varphi_{N+NB}\} \tag{23}$$

c) *Generalized Polynomial of chaos and stochastic Galerkin solution*

Assuming that the S_i^k represents a space of univariate orthonormal polynomial of variable $y_i \in \Gamma_i \subset \mathbb{R}$ with order k or lower and:

$$S_i^k = \{P_{a_i}^i(y_i), a_i = 1, 2, \dots, k\}, i = 1, \dots, M \quad (24)$$

The tensor product of the M S_i^k subspace results the space of the Generalized Polynomial Chaos:

$$S^k = S_1 \otimes S_2 \dots \otimes S_M \quad (25)$$

Xiu & Karniadakis (2003) show the application of the method for different kind of orthonormal polynomials and in the current paper the Hermite polynomial was used with the following characteristics:

$$P_0 = 1, \langle P_i \rangle = 0, i > 0 \quad (26)$$

Where:

$\gamma_n = \langle P_n^2 \rangle$: are the normalization factors.

δ_{mn} is the Kronecker delta

$$\rho(\mathbf{y}) = \frac{1}{\sqrt{2\pi}} e^{-\frac{x}{2}} \text{ is the density function} \quad (27)$$

And:

$$P_n = (-1)^n e^{\frac{x}{2}} \frac{d^n}{dx^n} e^{-\frac{x}{2}} \quad (28)$$

The function $u_t \in W^{hk}$ can be written as the summation of S^k polynomials base as

$$u_t(\mathbf{x}, \mathbf{y}) = \sum_{k=1}^P u_k(\mathbf{x}) \psi_k(\mathbf{y}) \quad (29)$$

According that and using the inner product of the weak form equation on each polynomial of the S^k base and get:

$$\begin{aligned} \langle LHS, \psi_p \rangle &= \langle \int_D \frac{\partial \sum \tilde{u}_i \varphi_i}{\partial t} \cdot \varphi_j(\mathbf{x}) dx, \psi_p \rangle = \\ &= \langle \sum_{i=1}^{nnode} \frac{d\tilde{u}_i}{dt} \int_D \varphi_i(\mathbf{x}) \cdot \varphi_j(\mathbf{x}) dx, \psi_p \rangle = \\ &= \langle \sum_{i=1}^{nnode} \frac{d}{dt} \left(\sum_{k=1}^P u_{ik}(\mathbf{t}, \mathbf{x}) \psi_k(\mathbf{y}) \right) \int_D \varphi_i(\mathbf{x}) \cdot \varphi_j(\mathbf{x}) dx, \psi_p \rangle = \\ &= \sum_{i=1}^{nnode} \sum_{k=1}^P \frac{du_{ik}(\mathbf{t}, \mathbf{x})}{dt} \psi_k(\mathbf{y}) \int_D \varphi_i(\mathbf{x}) \cdot \varphi_j(\mathbf{x}) dx, \psi_p \rangle = \\ &= \sum_{i=1}^{nnode} \sum_{k=1}^P \frac{du_{ik}(\mathbf{t}, \mathbf{x})}{dt} \int_{\Gamma} \rho(\mathbf{y}) \psi_k(\mathbf{y}) \psi_p(\mathbf{y}) \int_D \varphi_i(\mathbf{x}) \cdot \varphi_j(\mathbf{x}) dx dy = \\ &= \frac{du(\mathbf{t}, \mathbf{x})}{dt} \cdot M \otimes \langle \psi_k \psi_p \rangle \end{aligned} \quad (30)$$

Where:

$$M = \int_D \varphi_i(\mathbf{x}) \cdot \varphi_j(\mathbf{x}) dx \quad (31)$$

$$\langle \psi_k \psi_p \rangle = \int_{\Gamma} \rho(\mathbf{y}) \psi_k(\mathbf{y}) \psi_p(\mathbf{y}) dy \quad (32)$$

And the RHS of the weak form:

$$\begin{aligned}
 RHS >=< \int_D D_{if}(\mathbf{x}, \boldsymbol{\omega}) \nabla u(\mathbf{t}, \mathbf{x}, \boldsymbol{\omega}) \cdot \nabla v(\mathbf{x}) dx, \psi_p > - \\
 < \int_D c(\mathbf{x}, \boldsymbol{\omega}) \nabla u(\mathbf{t}, \mathbf{x}, \boldsymbol{\omega}) \cdot v(\mathbf{x}) dx, \psi_p > - \int_D f(\mathbf{x}, \boldsymbol{\omega}) \cdot v(\mathbf{x}) dx
 \end{aligned} \tag{33}$$

Set

$$I_1 = < \int_D D_{if}(\mathbf{x}, \boldsymbol{\omega}) \nabla u(\mathbf{t}, \mathbf{x}, \boldsymbol{\omega}) \cdot \nabla v(\mathbf{x}) dx, \psi_p > \tag{34}$$

$$I_2 < \int_D c(\mathbf{x}, \boldsymbol{\omega}) \nabla u(\mathbf{t}, \mathbf{x}, \boldsymbol{\omega}) \cdot v(\mathbf{x}) dx, \psi_p > \tag{35}$$

And let calculate these two integrals:

$$\begin{aligned}
 I_1 &=< \int_D D_{if}(\mathbf{x}, \boldsymbol{\omega}) \nabla u(\mathbf{t}, \mathbf{x}, \boldsymbol{\omega}) \cdot \nabla v(\mathbf{x}) dx, \psi_p > = \\
 < \int_D D_{if}(\mathbf{x}, \boldsymbol{\omega}) \sum_1^{nnode} u_i(\mathbf{t}, \mathbf{x}, \boldsymbol{\omega}) \cdot \nabla \varphi_i(\mathbf{x}) \nabla \varphi_j(\mathbf{x}) dx, \psi_p > = \\
 < \sum_1^{nnode} u_i(\mathbf{t}, \mathbf{x}, \boldsymbol{\omega}) \int_D D_{if}(\mathbf{x}, \boldsymbol{\omega}) \cdot \nabla \varphi_i(\mathbf{x}) \nabla \varphi_j(\mathbf{x}) dx, \psi_p > = \\
 < \sum_1^{nnode} \sum_k^P u_i(\mathbf{t}, \mathbf{x}) \boldsymbol{\psi}_k(\mathbf{y}) \int_D D_{if}(\mathbf{x}, \boldsymbol{\omega}) \cdot \nabla \varphi_i(\mathbf{x}) \nabla \varphi_j(\mathbf{x}) dx, \psi_p > = \\
 < \sum_1^{nnode} \sum_k^P u_i(\mathbf{t}, \mathbf{x}) \boldsymbol{\psi}_k(\mathbf{y}) \int_D e^{\overline{D}_{if}(\mathbf{x}) + \sum_{\kappa=1}^K \sqrt{\lambda_{\kappa}} \varphi_{\kappa} \xi_{\kappa}(\mathbf{y})} \cdot \nabla \varphi_i(\mathbf{x}) \nabla \varphi_j(\mathbf{x}) dx, \psi_p > = \\
 < \sum_1^{nnode} \sum_k^P u_{ik}(\mathbf{t}, \mathbf{x}) \boldsymbol{\psi}_k(\mathbf{y}) e^{\sum_{\kappa=1}^K \sqrt{\lambda_{\kappa}} \varphi_{\kappa} \xi_{\kappa}(\mathbf{y})} \int_D e^{\overline{D}_{if}(\mathbf{x})} \cdot \nabla \varphi_i(\mathbf{x}) \nabla \varphi_j(\mathbf{x}) dx, \psi_p > = \\
 \sum_1^{nnode} \sum_k^P u_{ik}(\mathbf{t}, \mathbf{x}) \int_{\Gamma} \rho(\mathbf{y}) e^{\sum_{\kappa=1}^K \sqrt{\lambda_{\kappa}} \varphi_{\kappa} \xi_{\kappa}(\mathbf{y})} \boldsymbol{\psi}_k(\mathbf{y}) \boldsymbol{\psi}_p(\mathbf{y}) \int_D e^{\overline{D}_{if}(\mathbf{x})} \cdot \nabla \varphi_i(\mathbf{x}) \nabla \varphi_j(\mathbf{x}) dx dy = \\
 K \otimes < e^{G(\xi)} \boldsymbol{\psi}_k(\mathbf{y}) \boldsymbol{\psi}_p(\mathbf{y}) > \tilde{u}(\mathbf{t}, \mathbf{x})
 \end{aligned} \tag{36}$$

Where

$$K = \int_D e^{\overline{D}_{if}(\mathbf{x})} \cdot \nabla \varphi_i(\mathbf{x}) \nabla \varphi_j(\mathbf{x}) dx \tag{37}$$

$$< e^{G(\xi)} \boldsymbol{\psi}_k(\mathbf{y}) \boldsymbol{\psi}_p(\mathbf{y}) > = \int_{\Gamma} \rho(\mathbf{y}) e^{\sum_{\kappa=1}^K \sqrt{\lambda_{\kappa}} \varphi_{\kappa} \xi_{\kappa}(\mathbf{y})} \boldsymbol{\psi}_k(\mathbf{y}) \boldsymbol{\psi}_p(\mathbf{y}) d\mathbf{y} \tag{38}$$

Thus

$$I_1 = K \otimes \langle e^{G(\xi)} \psi_k(\mathbf{y}) \psi_p(\mathbf{y}) \rangle \tilde{u}(t, x) \tag{39}$$

And

$$\begin{aligned}
 I_2 &= \langle \int_D c(\mathbf{x}, \boldsymbol{\omega}) \nabla u(\mathbf{t}, \mathbf{x}, \boldsymbol{\omega}) \cdot v(\mathbf{x}) dx, \psi_p \rangle \\
 &= \langle \int_D c(\mathbf{x}, \boldsymbol{\omega}) \sum_i^{nnode} u_i(\mathbf{t}, \mathbf{x}, \boldsymbol{\omega}) \cdot \nabla \varphi_i(\mathbf{x}) \varphi_j(\mathbf{x}) dx, \psi_p, \psi_p \rangle \\
 &= \langle \sum_i^{nnode} u_i(\mathbf{t}, \mathbf{x}, \boldsymbol{\omega}) \int_D c(\mathbf{x}, \boldsymbol{\omega}) \cdot \nabla \varphi_i(\mathbf{x}) \varphi_j(\mathbf{x}) dx, \psi_p \rangle = \\
 &= \langle \sum_i^{nnode} \sum_k^P u_i(\mathbf{t}, \mathbf{x}) \psi_k(\mathbf{y}) \int_D c(\mathbf{x}, \boldsymbol{\omega}) \cdot \nabla \varphi_i(\mathbf{x}) \varphi_j(\mathbf{x}) dx, \psi_p \rangle = \\
 &= \langle \sum_i^{nnode} \sum_k^P u_i(\mathbf{t}, \mathbf{x}) \psi_k(\mathbf{y}) \int_D e^{\tilde{c}(\mathbf{x}) + \sum_{\kappa=1}^K \sqrt{\lambda_{\kappa}} \varphi_{\kappa} \xi_{\kappa}(\mathbf{y})} \cdot \nabla \varphi_i(\mathbf{x}) \varphi_j(\mathbf{x}) dx, \psi_p \rangle = \\
 &= \langle \sum_i^{nnode} \sum_k^P u_{ik}(\mathbf{t}, \mathbf{x}) \psi_k(\mathbf{y}) e^{\sum_{\kappa=1}^K \sqrt{\lambda_{\kappa}} \varphi_{\kappa} \xi_{\kappa}(\mathbf{y})} \int_D e^{\tilde{c}(\mathbf{x})} \cdot \nabla \varphi_i(\mathbf{x}) \varphi_j(\mathbf{x}) dx, \psi_p \rangle = \\
 &= \sum_i^{nnode} \sum_k^P u_{ik}(\mathbf{t}, \mathbf{x}) \int_{\Gamma} \rho(\mathbf{y}) e^{\sum_{\kappa=1}^K \sqrt{\lambda_{\kappa}} \varphi_{\kappa} \xi_{\kappa}(\mathbf{y})} \psi_k(\mathbf{y}) \psi_p(\mathbf{y}) \int_D e^{\tilde{c}(\mathbf{x})} \cdot \nabla \varphi_i(\mathbf{x}) \varphi_j(\mathbf{x}) dx dy = \\
 C \otimes \langle e^{G(\xi)} \psi_k(\mathbf{y}) \psi_p(\mathbf{y}) \rangle \tilde{u}(t, x) \tag{40}
 \end{aligned}$$

Where

$$C = \int_D e^{\tilde{c}(\mathbf{x})} \cdot \nabla \varphi_i(\mathbf{x}) \varphi_j(\mathbf{x}) dx \tag{41}$$

Based on the above the initial equation of the transport phenomena under random behavior is equal to

$$\begin{aligned}
 \frac{du(\mathbf{t}, \mathbf{x})}{dt} \cdot M \otimes \langle \psi_k \psi_p \rangle &= K \otimes \langle e^{G(\xi)} \psi_k(\mathbf{y}) \psi_p(\mathbf{y}) \rangle \tilde{u}(t, x) \\
 - C \otimes \langle e^{G(\xi)} \psi_k(\mathbf{y}) \psi_p(\mathbf{y}) \rangle &\tilde{u}(t, x) - f(t, x) \tag{42}
 \end{aligned}$$

To solve this system there are various schemes to use and in the current paper the backward Euler method was applied:

$$\begin{aligned}
 \frac{d\tilde{u}}{dt} \cdot M \otimes \langle \psi_k \psi_p \rangle &= K \otimes \langle e^{G(\xi)} \psi_k(\mathbf{y}) \psi_p(\mathbf{y}) \rangle \tilde{u}_{t_{n+1}} \\
 - C \otimes \langle e^{G(\xi)} \psi_k(\mathbf{y}) \psi_p(\mathbf{y}) \rangle &\tilde{u}_{t_{n+1}} - f \tag{43}
 \end{aligned}$$

Set

$$MP = M \otimes \langle \psi_k \psi_p \rangle \tag{44}$$

$$KP = K \otimes \langle e^{G(\xi)} \psi_k(\mathbf{y}) \psi_p(\mathbf{y}) \rangle \tag{45}$$

$$CP = C \otimes \langle e^{G(\xi)} \psi_k(\mathbf{y}) \psi_p(\mathbf{y}) \rangle \tag{46}$$

$$\frac{d\tilde{u}}{dt} \cdot MP = KP\tilde{u}_{t_{n+1}} - CP\tilde{u}_{t_{n+1}} - f \tag{47}$$

After some algebra:

$$\tilde{u}_{t_{n+1}} = \frac{MP\tilde{u}_{t_n} - \Delta t \cdot f}{MP - \Delta t(KP - CP)} \tag{48}$$

The statistical moments of the displacement field arise by the properties of the Polynomial of Chaos expansion:

The expected value

$$\underbrace{u_0(\mathbf{x})\mathbb{E}[\psi_0(\mathbf{y})]}_1 + \underbrace{\sum_{k=1}^P u_k(\mathbf{x})\mathbb{E}[\psi_k(\mathbf{y})]}_0 = u_0(\mathbf{x}) \tag{49}$$

And the variance

$$\begin{aligned} \sigma^2 &= \mathbb{E}(u(\mathbf{x}, \mathbf{y}) - \mathbb{E}[u(\mathbf{x}, \mathbf{y})])^2 = \\ &\mathbb{E}\left(\sum_{k=0}^P u_k(\mathbf{x})\mathbb{E}[\psi_k(\mathbf{y})] - u_0(\mathbf{x})\right) \Rightarrow \\ \sigma^2 &= \sum_{k=0}^P u_k^2(\mathbf{x})\mathbb{E}[\psi_k^2] \end{aligned} \tag{50}$$

V. NUMERICAL EXAMPLE

Considering a point source of pollution and the need to estimate its progress due to diffusion and advection phenomena. The problem and the geometry of the finite elements used presented in figure 10. The advection coefficient for simplicity is assumed to be deterministic and constant where the diffusion coefficient present spatial randomness and it is simulated as a random field (figure 11).

To solve the problem the application of the numerical algorithms described in the previous paragraphs is presented and results are compared to those obtained from RFEM using Monte Carlo simulations. The dimensionless input data of the problem is the random field diffusion coefficient with a constant average value equal to 0.1 and a fixed advection coefficient equal to 0.1. An initial source of

point pollution equal to 2 is applied as described in figure 10.

In the figures 12-14 the two methods results of the expected values and standard deviation of concentration are shown for variation coefficient $v_e = 0.4$ and number of Monte Carlo samples for the RFEM equal to 1000.

The problem then was solved for three different number of Monte Carlo samples for the RFEM and 5, 50, 500 simulations are executed creating 10, 100, and 1000 realisation while for SFEM were used one dimensional Hermite GPC with order 3 (Xiu & Karniadakis 2003). Calculations have been made for twelve different coefficients $v_e = \frac{\sigma_E}{\mu_E}$ of the diffusion coefficient with a minimum value of 0.1 and then with step 0.1 to a maximum value equal to 1.2.

In figures 14, 15 the results for the various calculation are presented. It is observed that as the number of sample increase the results of the Monte Carlo convergence to GPC method and for number of samples equal to 1000 a great accuracy is presented. In figures 17 and 18 this reduction is shown for a variation coefficient $v_e = 0.5$.

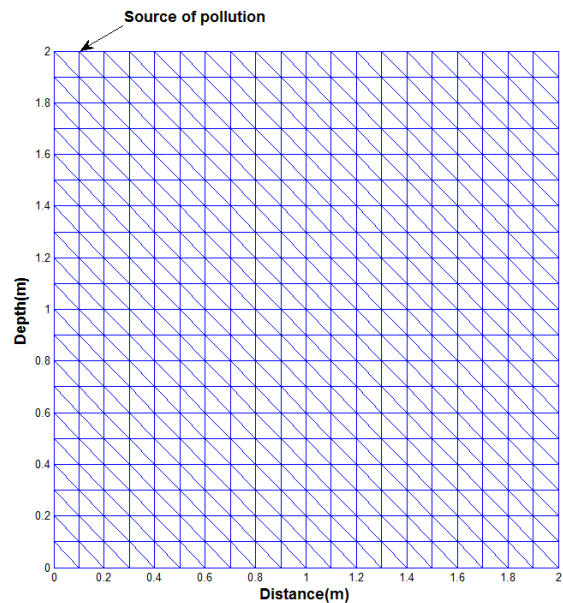


Figure 10 : Finite element mesh

Realisation of Diffusion Coefficient

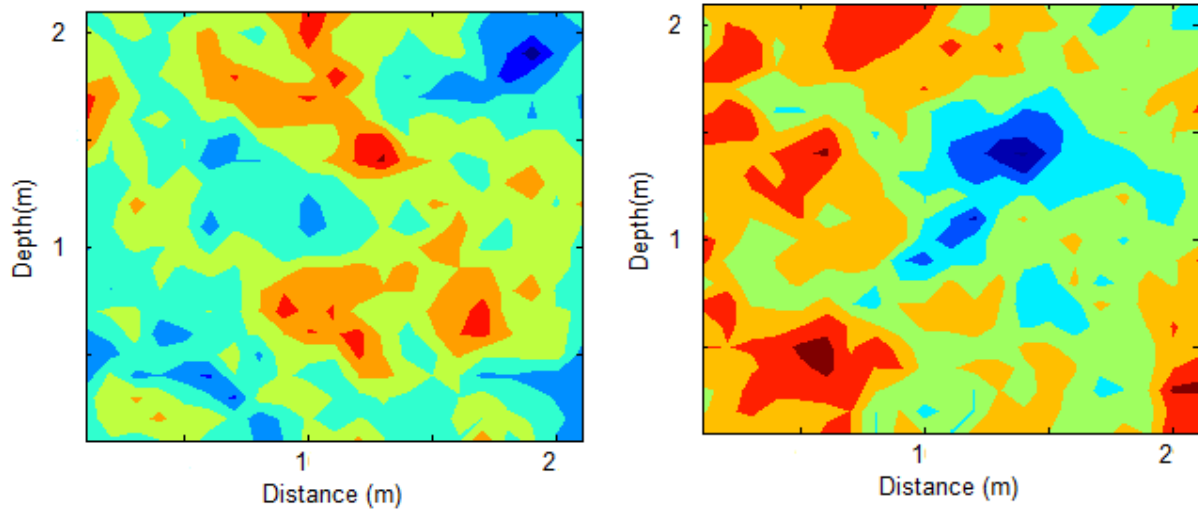


Figure 11 : Realisation of Diffusion Coefficient

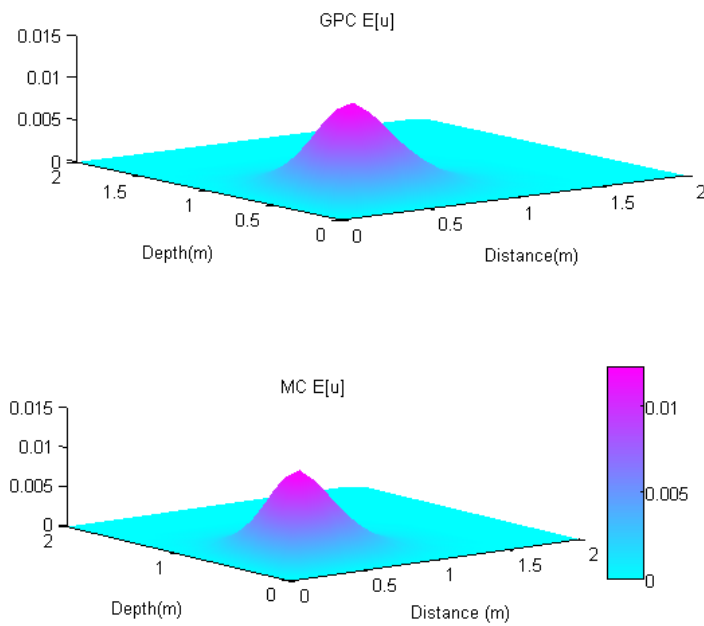


Figure 12 : Expected value of concentration at time 3dt



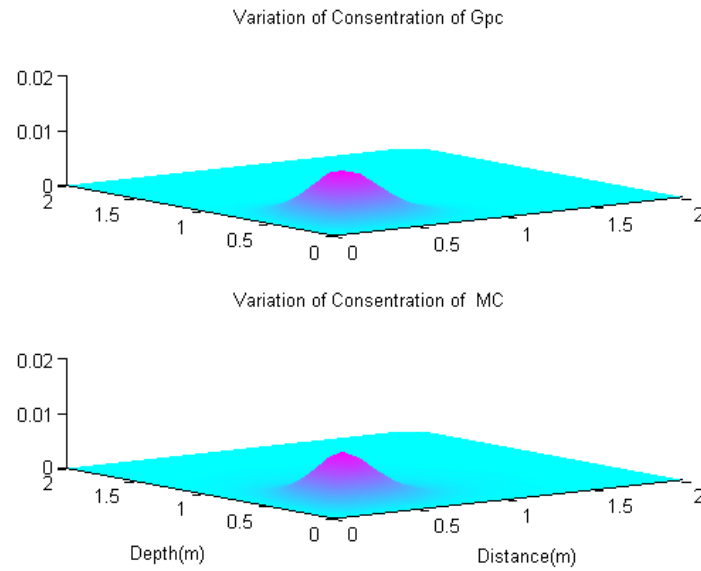


Figure 13 : Standard deviation of concentration at time 3dt

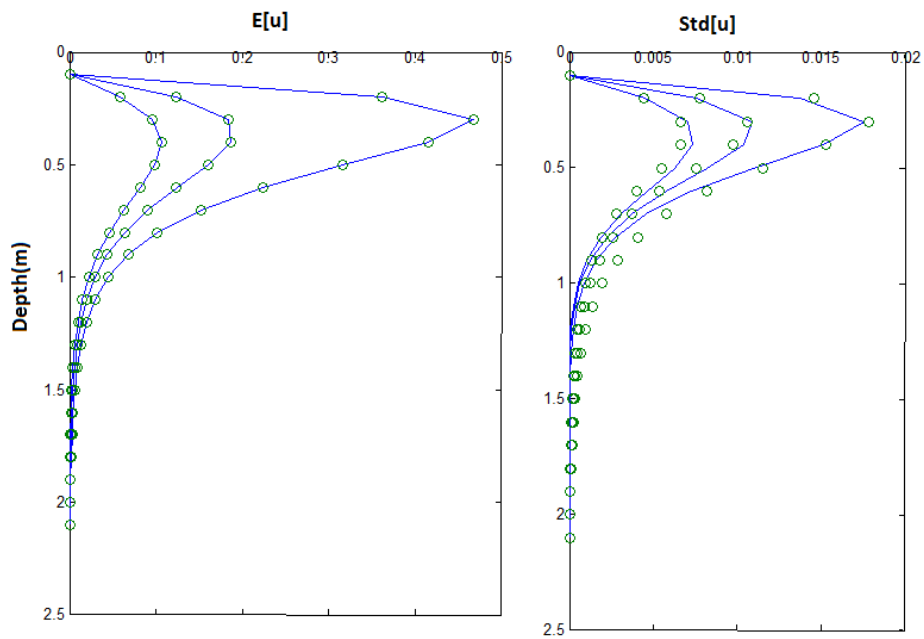


Figure 14 : Expected value and Standard deviation of concentration for tree different times (Standard deviation of diffusion coefficient $\sigma=0.4$)



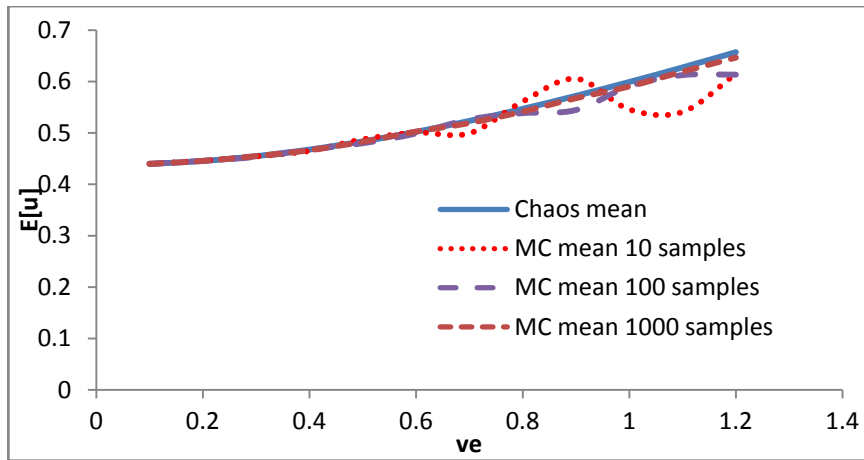


Figure 15 : Results of the expected value for twelve different values of variation coefficient and for tree different sample's number of Monte Carle method

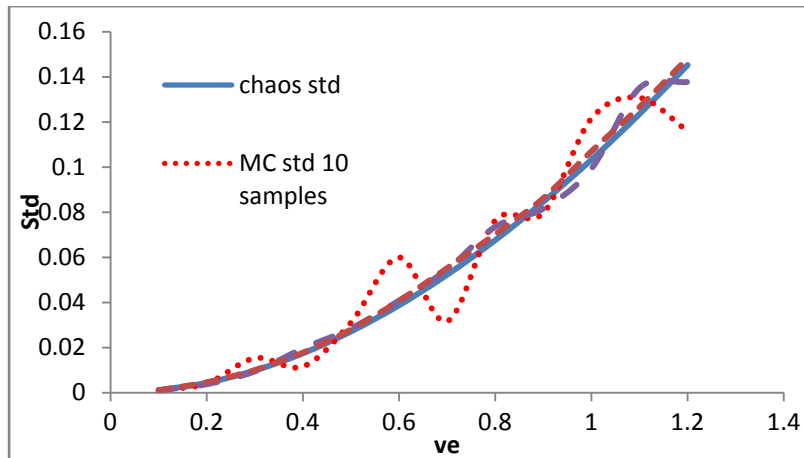


Figure 16 : Results of standard deviation of concentration for twelve different values of variation coefficient and for tree different sample's number of Monte Carle method

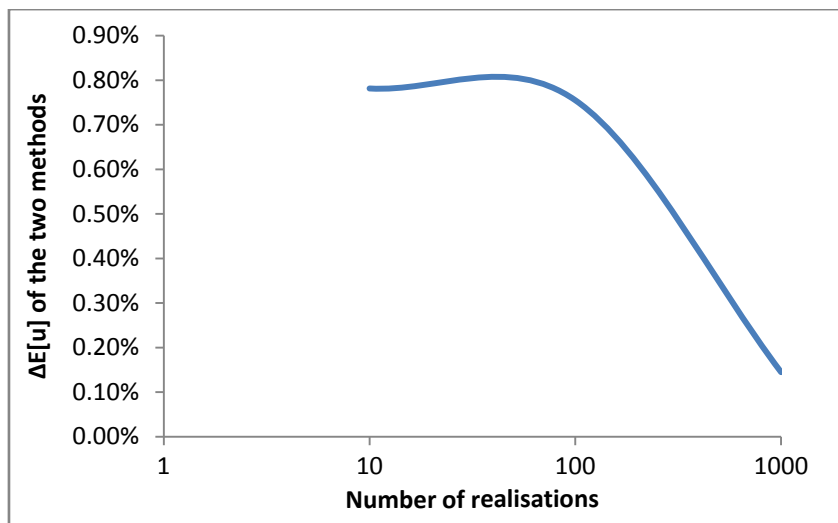


Figure 17 : Expected value different of the two methods for various numbers of realisations and for variation coefficient equal to 0.5

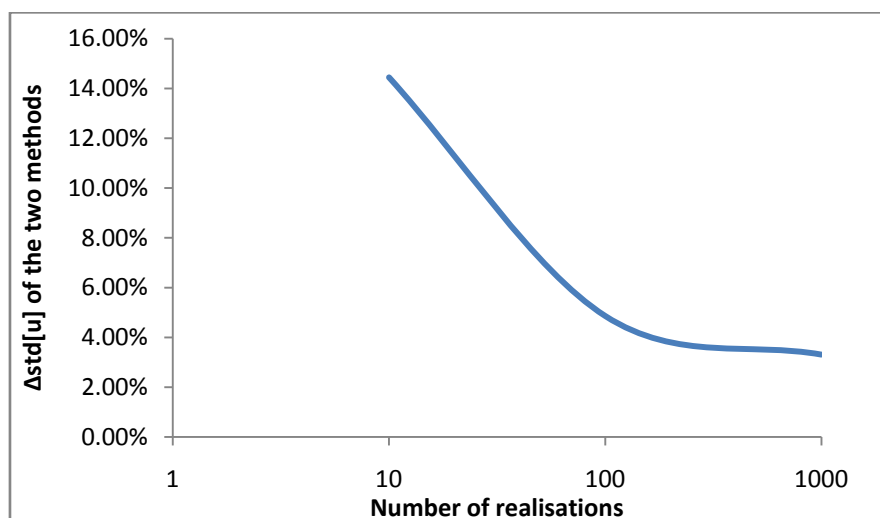


Figure 18 : Standard deviation different of the two methods for various numbers of realizations and for variation coefficient equal to 0.5

VI. CONCLUSIONS

A procedure of conducting a Stochastic Finite Element Analysis of Transport phenomena in Geomechanics where uncertainty arises due to spatial variability of mechanical parameters of soil/rock has been presented. Two different approaches in order to quantifying uncertainty are discussed. The first approach involves generating a random field based on Circulant embedding method and the second Stochastic Finite Element using Polynomial Chaos. A problem of a point source of pollution its progress due to diffusion and advection phenomena used to show the application of the methods.

It is shown that the results of SFEM using polynomial chaos compare well with those obtained from Random Finite Element Method. The main advantage in using the proposed methodology is that a large number of realisations which have to be made for RFEM are avoided, thus making the procedure viable for realistic practical problems.

REFERENCES RÉFÉRENCES REFERENCIAS

- Zhang, P. and Hu, L. (2014) Contaminant Transport in Soils Considering Preferential Flowpaths. *Geoenvironmental Engineering*: pp. 50-59.
- Mousavi Nezhad, M., Javadi, A., Al-Tabbaa, A., and Abbasi, F. (2013). "Numerical study of soil heterogeneity effects on contaminant transport in unsaturated soil (model development and validation)." *International Journal for Numerical and Analytical Methods in Geomechanics*.
- Johnson, B., Elmore, A., and Cawfield, J. (2010). "Application of a Mass Balance-Based Stochastic Transport Model." *Pract. Period. Hazard. Toxic Radioact. Waste Manage.*, 14(3), 170–177.
- Nadim K. Coptly, Didar Ergene, and Turgut T. Onay (2004) "Stochastic Model for Landfill Gas Transport and Energy Recovery" *Journal of Environmental Engineering* Sep2004, Vol. 130, No. 9, pp. 1042-1049.
- Wörman, A. and Xu, S. (2001). "Stochastic Analysis of Internal Erosion in Soil Structures-Implications for Risk Assessments." *J. Hydraul. Eng.*, 127(5), 419–428.
- Davies, R. & Harte, D. (1987), "Tests for Hurst effect", *Biometrika* 74(4), 95–101.
- Dembo, A., Mallows, C. & Shepp, L. (1989), "Embedding nonnegative definite Toeplitz matrices in nonnegative definite circulant matrices, with applications to covariance estimation", *IEEE Transactions on Information Theory* 35, 1206–1212.
- Dietrich, C. & Newsam, G. (1993), "A fast and exact simulation for multidimensional Gaussian stochastic simulations", *Water Resources Research* 29(8), 2861–2869.
- Dietrich, C. & Newsam, G. (1997), "Fast and exact simulation of stationary Gaussian processes through circulant embedding of the covariance matrix", *SIAM Journal on Scientific Computing* 18(4), 1088–1107.
- Gneiting, T. (2000), "Power-law correlations, related models for long-range dependence and their simulation", *Journal of Applied Probability* 37(4), 1104–1109.
- Gneiting, T., Ševčíková, H., Percival, D., Schlather, M. & Jiang, Y. (2006), "Fast and exact simulation of large Gaussian lattice systems in R2: Exploring the limits", *Journal of Computational and Graphical Statistics* 15(3), 483–501.
- Stein, M. (2001), "Local stationarity and simulation of self-affine intrinsic random functions", *IEEE*

Transactions on Information Theory 47(4), 1385–1390.

13. Stein, M. (2002), “Fast and exact simulation of fractional Brownian surfaces”, Journal of Computational and Graphical Statistics 11(3), 587–599.

14. Stein, M. (2012), “Simulation of Gaussian random fields with one derivative”, Journal of Computational and Graphical Statistics 21(1), 155–173.

15. Wood, A. & Chan, G. (1994), “Simulation of stationary Gaussian processes in $[0, 1]^d$ ”, Journal of Computational and Graphical Statistics 3(4), 409–432.

16. Ghanem, R. G., and Spanos, P. D. 1991. Stochastic finite elements: A spectral approach, Springer-Verlag, New York.

17. D Xiu, G Em Karniadakis. 2003 “Modeling uncertainty in steady state diffusion problems via generalized polynomial chaos” Computer Methods in Applied Mechanics and Engineering 191 (43), 4927-4948.

18. Robert M. Gray 2006 “Toeplitz and Circulant Matrices: A review” Department of electrical Engineering Stanford University.

APPENDIX A

Definition 1. A Toeplitz matrix is an $n \times n$ matrix $T_n = [t_{k,j} : k, j = 0, 1, \dots, n - 1]$ where $t_{k,j} = t_{k-j}$, i.e., a matrix of the form:

$$T_n = \begin{bmatrix} t_0 & t_{-1} & t_{-1} & \dots & t_{-(n-1)} \\ t_1 & t_0 & t_{-1} & & \vdots \\ t_2 & t_1 & t_0 & & \\ \vdots & & & \ddots & \\ t_{n-1} & & & \dots & t_0 \end{bmatrix}$$

Definition 2. When every row of the matrix is a right cyclic shift of the row above it so that $t_k = t_{-(n-k)}$ for $k = 1, 2, \dots, n - 1$. In this case the matrix is called Circulant and is equal to:

$$C_n = \begin{bmatrix} t_0 & t_{-1} & t_{-2} & \dots & t_{-(n-1)} \\ t_{-(n-1)} & t_0 & t_{-1} & & \vdots \\ t_{-(n-2)} & t_{-(n-1)} & t_0 & & \\ & & & \ddots & \\ t_{-1} & t_{-2} & & \dots & t_0 \end{bmatrix}$$

Definition 3. If C_k is $n_1 \times n_1$ Toeplitz matrix then the $N \times N$ matrix with $N = n_1 n_2$ and the form:

$$C = \begin{bmatrix} C_0 & C_{-1} & \dots & C_{2-n_2} & C_{1-n_2} \\ C_1 & C_0 & C_{-1} & \ddots & C_{2-n_2} \\ \vdots & \ddots & \ddots & & \vdots \\ C_{n_2-2} & \ddots & C_1 & C_0 & C_{-1} \\ C_{n_2-1} & C_{n_2-2} & \dots & C_1 & C_0 \end{bmatrix}$$

is called Block Toeplitz matrix with Toeplitz Blocks (BTTB).